Gas bearing slumping and figure correction of X-ray telescope mirror substrates

Brandon Chalifoux*[a], Heng Zuo[a], Graham Wright[b], Youwei Yao[a],
Ralf K. Heilmann[c], Mark L. Schattenburg[c]
[a]Dept. of Mechanical Engineering, MIT, Cambridge, MA, USA 02139
[b]Plasma Science and Fusion Center, MIT, Cambridge, MA, USA 02139
[c]Space Nanotechnology Lab, MIT Kavli Institute, Cambridge, MA, USA 02139
*bchal@mit.edu; phone: (617) 253-3130; fax: (617) 452-2888; snl.mit.edu

ABSTRACT

Figure correction of thin x-ray telescope mirrors may be critical for future missions that require high angular resolution and large collecting areas. One promising method of providing figure correction is to use stress generated via ion implantation. Since stress-based figure correction strategies cannot correct high spatial frequency errors, it is critical to obtain glass with only low spatial frequency error. One method is thermal gas bearing slumping, where glass is softened while floating on thin films of gas. This method avoids introducing mid- or high- spatial frequency errors by eliminating contact between the glass and mandrel. Together, these two methods form a promising approach to fabricating mirrors for a high angular resolution, large-area x-ray observatory. In this paper we report on progress in understanding gas bearing slumping, and advancing the technology to curved geometry. We also report on continued progress on advancing the ion implantation technology toward correcting flight-sized mirror substrates.

Keywords: X-ray mirrors, slumping, thermo-forming, figure correction, ion implantation, glass

1. INTRODUCTION

The X-ray surveyor mission concept calls for a sub-arcsecond half-power diameter (HPD) angular resolution with 30 times greater effective area than the Chandra X-ray Observatory[1]. This requires thin mirrors that are far more accurate than have been made to date. One potential route to fabricating highly accurate thin mirrors is to form a substrate close to the desired shape, then if necessary, correct as much of the residual error as possible.

Forming a substrate with good figure may be achieved by slumping glass[2,3,4,5], or grinding and polishing silicon[2]. Error correction may potentially be achieved using either stress-based methods to bend the substrate to the desired shape (e.g., magneto-strictive films[6], ion implantation[7], or piezoelectric films[5]); or direct methods, such as differential deposition[8,9], to remove/add material to achieve the desired surface height. In the current work, we focus on gas bearing slumping[3] to form the substrate, followed by ion implantation figure correction[7] to bend the substrate to remove residual figure errors.

All stress-based figure correction methods rely on changing the curvature of the substrate. As a useful approximation, the correction stress approximately scales with the required changes in curvature. In addition, low spatial frequency axial slope error is the dominant term contributing to the telescope point-spread function. For a given magnitude of correction stress that may be applied, more error is correctable if the mirror slope errors are dominated by low spatial-frequencies. This is the goal of gas bearing slumping: to form glass substrates dominated by low spatial-frequency errors, but that are close enough to the desired figure to be correctable with stress-based methods, in particular, ion implantation figure correction.

Space Telescopes and Instrumentation 2016: Ultraviolet to Gamma Ray, edited by
Jan-Willem A. den Herder, Tadayuki Takahashi, Marshall Bautz, Proc. of SPIE Vol. 9905, 990522
· © 2016 SPIE · CCC code: 0277-786X/16/$18 · doi: 10.1117/12.2232500

Gas bearing slumping operates by forcing gas (typically nitrogen) through a porous mandrel, where it flows into a thin ~50 μm gap between the mandrel and glass, and a pressure field develops beneath the glass that supports it. Mandrels are used on both sides of the glass, and as the entire assembly is heated and the glass softens, it is forced to approximately replicate the shape of the mandrels. This process is illustrated in Figure 1. The details of the sensors, actuators, and control systems have been reported previously[3]. We have made recent progress in understanding the gas bearing slumping process better through modeling; this information will inform the design of a curved gas bearing slumping tool. The modeling effort will be detailed in Section 2.

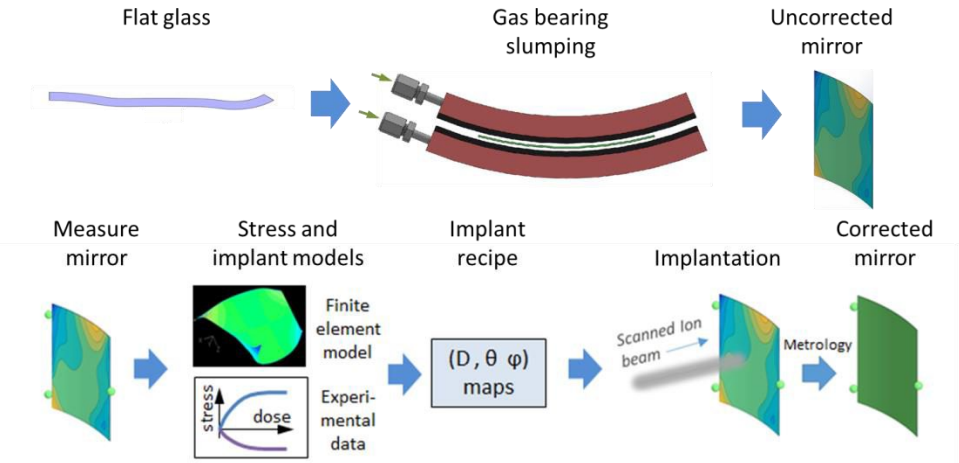

Figure 1. Gas bearing slumping and ion implantation figure correction processes.

Ion implantation figure correction works by creating thermal spikes (for more information on this phenomena, see the review by Klaumünzer[10]) within an amorphous material such as glass, which results in a build-up stress near the surface of the substrate. While this phenomenon has been observed in many amorphous materials[10], our recent work has focused on implanting 6 MeV O^{3+} ions into Schott D-263 glass, which results in an implant depth of 3.5 μm. This particular material and ion species and energy is attractive because we are able to achieve a highly non-equibiaxial stress that depends on the ion beam orientation relative to the substrate. We have previously detailed how this may be used for figure correction[7]. We may control the direction of stress (i.e., the relative magnitudes of x, y, and shear components) by controlling the ion beam angles, and we may control the magnitude and location of the stress via the ion dose at each location on the substrate.

We have recently completed building a sample stage and vacuum chamber that interfaces with a MeV ion accelerator located at the Massachusetts Institute of Technology (MIT). This system is currently capable of implanting samples up to 100 mm x 100 mm in size and will be described in detail in Section 3. Modifications to the ion beam line would allow implantation of larger substrates. In addition, this system will allow us to conduct in-situ curvature measurements at more angles of incidence, providing more complete data to validate or in-validate models.

2. MODELING GAS BEARING SLUMPING

Modeling the gas bearing slumping process is critical for designing and building a curved-substrate slumping tool that will produce substrates good enough to correct with ion implantation figure correction. Our current work has been focused on developing a good model that agrees with experimental results from our flat gas bearing slumping tool[3]. Once the reliability of this model is improved and confirmed, we intend to extrapolate this model to find geometric and

mandrel material properties that we expect to yield smaller residual figure errors. For example, we expect decreasing the bearing permeability to improve the mirror figure.

Gas bearing slumping is a good process for modeling because coulomb-type friction, which is typically difficult to model well, is absent since the glass is supported by gas films on both sides. Modeling difficulty arises because there is strong fluid-structure interaction; as the glass changes shape, the pressure distribution in the fluid gap also changes. The visco-elastic nature of softened glass also presents modeling challenges.

We are using a method of iterative relaxation to simulate the forming of a material with a very low shear modulus (such as softened glass), while keeping the model stable. This method is described in detail in Section 2.1. In this method, we simulate the coupled fluid-structure interaction between the gas and glass with a chosen starting shape and relatively high elastic moduli. We then find the glass vertical position within the bearings such that the net pressure on the glass is small. We then repeat the fluid-structure interaction with an updated glass shape and vertical position. After hundreds of iterations, the glass shape changes by a few nanometers, and the residual stress in the glass becomes small, as expected when approaching a steady state. However, we have also found that after many more iterations, changes in glass begin to develop rapidly; this is still under investigation.

We have compared the glass shapes predicted by the model to actual slumped flat substrates, and we find that there is relatively good agreement between the two. However, there is disagreement between the model and experiment for very long slumping times. These results are described in Section 2.2.

2.1 Iterative relaxation method

In this work, we are using ADINA to compute the pressure field in the gas film, as well as fluid-structure interaction results. Due to computational simplicity, we consider a 2-dimensional problem, with cylindrical symmetry. Figure 2 shows the geometry of the model. On the left side of the image is the axis of symmetry. The parameters for our current system, and the model, are listed in Table 1. The meshes for both the solid and fluid models are composed of 9-node 2-D axisymmetric elements (quadratic interpolation functions). The mesh parameters (included in Table 1) were chosen based on convergence testing and comparison with an analytical model; for 9-node elements, this requires very few radial and axial elements.

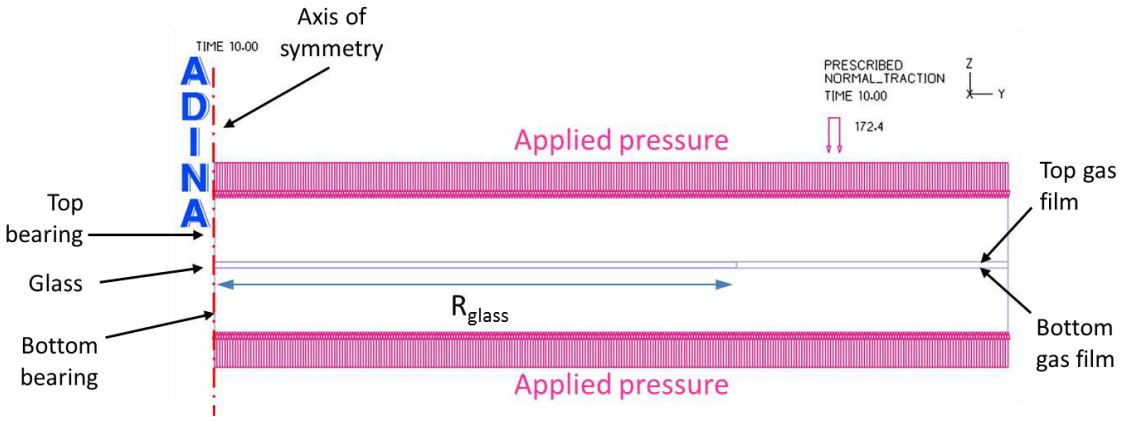

Figure 2. Slumping model geometry. The values of the model parameters used are listed in Table 1.

Table 1. Parameters used in slumping model in the current work.

Geometry parameters	**Value**
Glass radius	50 mm
Bearing radius	76.2 mm
Glass thickness	550 μm
Bearing thickness	6.35 mm
Nominal gap thickness (per side)	50 μm
Material parameters	
Glass Young's modulus*	72.9 GPa
Glass Poisson's ratio*	0.208
Bearing permeability	4×10^{-13} m^2
Fluid density (N_2 at 550 °C)	0.4037 kg/m^3
Fluid viscosity (N_2 at 550 °C)	3.62×10^{-5} Pa-sec
Mesh parameters	
Element type (same in gas film, bearing, and glass)	9-node axisymmetric (quadratic interpolation)
Radial elements (same in gas film, bearing, and glass)	64
Axial elements, bearing	16
Axial elements, gas film	16
Axial elements, glass	2

* These values are used for each fluid-structure interaction iteration, but iterative relaxation reduces the effective Young's modulus to near-zero.

The center boundary of the glass is held fixed in both the radial and axial directions, to speed up the fluid-structure interaction problem. However, the height of the glass will quickly float to a location where the net force (including gravity) is zero. Therefore, the first step in this model is to find the vertical position of the glass before solving the fluid-structure interaction problem. This is accomplished by calculating the pressure field using ADINA, calculating the net force on the glass, moving the glass position slightly, and repeating these steps until the net force on the glass is very small ($< 10^{-6}$ N).

The second step is to calculate the change in shape of the glass, given a starting glass shape. The solid and fluid models are iteratively solved in ADINA until the net force on each node in the glass converges. This part of the model is not stable if the Young's modulus of the glass is too small, because in that case, small force imbalances result in large deformations. These large deformations result in instability, potentially because of the highly nonlinear change in fluid pressure with gap thickness. However, using a sufficiently large number of iterations, we expect the result to be the same when using a room-temperature Young's modulus as using a low Young's modulus.

The glass shape is then updated, and the two steps are repeated with the new glass shape. An example of the progression of glass shapes is shown in Figure 3.

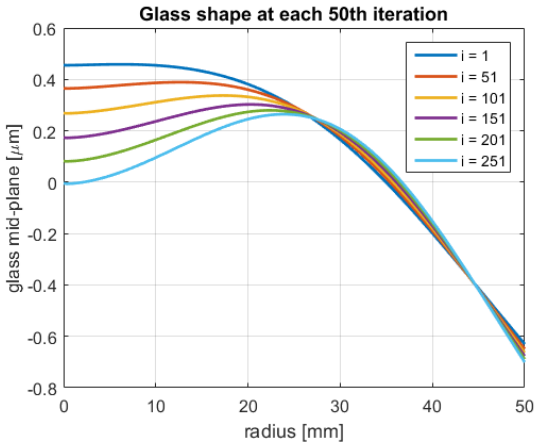

Figure 3. An example of glass shape progression at different iterations.

2.2 Comparison with experiment

In order to make design decisions based on our slumping model, it is critical that this model agree with the current slumping tool, at least. In general, we have found this to be the case, as shown in Figure 5. Figure 4 shows a typical slumped glass surface figure measurement, for a slumping temperature of 550 °C, a ramp time of 3 hours, and a dwell time of 16 hours. In Figure 5, the scatter points are the measured slumped wafer surface, collapsed onto a radius vs. height plot.

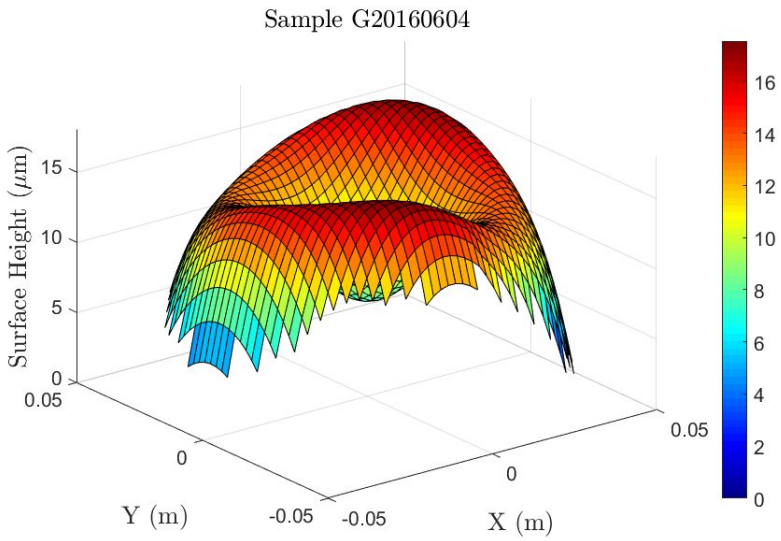

Figure 4. A typical slumped glass sample. This sample was slumped at 550 °C for 16 hours.

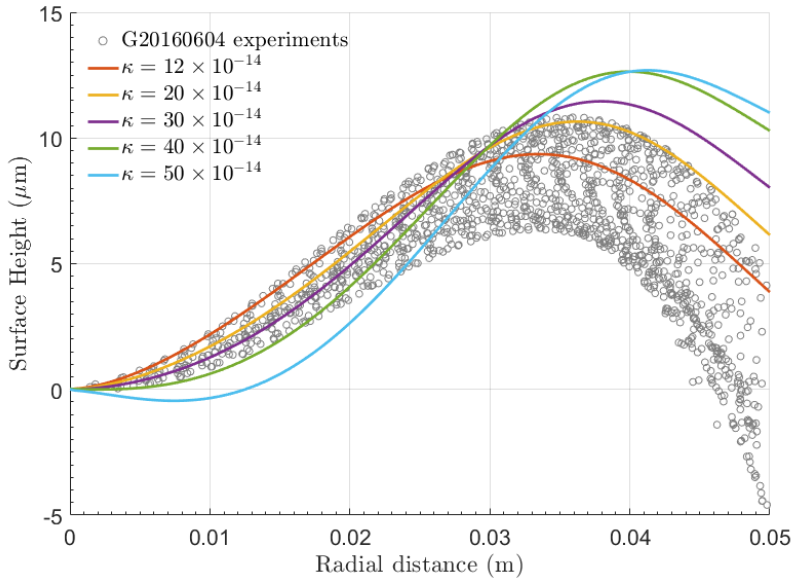

Figure 5. Modeled glass shapes compared with the sample shown in Figure 4. The measured bearing permeability was 40 x 10^{-14} m^2. This figure also illustrates the beneficial effect of reducing bearing permeability.

The general shape of the glass is predicted by the model. From this plot it is also clear that the permeability of the bearing is expected to significantly affect the glass shape, with smaller permeability resulting in better figure. The silicon carbide bearings we are currently using have a permeability ~100x larger than typical graphite air bearings.

While 8 hours of slumping at 550 °C appears to qualitatively agree with the model, when we slump samples for 100 hours, there is continued degradation of the glass figure, into a large dome that is not measureable with our Shack-Hartmann metrology system[11]. For large numbers of iterations, the model also appears to continue changing at a slow rate, but such that it is not consistent with the experimental results. We are continuing to develop and test this model to ensure it agrees with experimental results.

We expect that a low-porosity graphite air bearing will provide lower figure errors in the glass, so we will investigate this further in the model. The challenge with graphite is that it degrades when heated to >450 °C in the presence of oxygen; we are currently measuring how much oxygen is tolerable so we can build a long-lasting graphite air bearing.

3. ION IMPLANTATION SYSTEM

In order to test the effectiveness of using ion implantation for figure correction of thin x-ray mirrors, we must be able to control the ion dose, location, and direction over the surface of a substrate. Controlling ion dose may be achieved by measuring the total number of charges hitting the sample, by integrating the current passing from the sample to ground and dwelling at a particular location until the desired dose is achieved. Controlling the location of the ion beam on the sample may be achieved by electrostatically deflecting the ion beam. Controlling the direction of the ion beam relative to the sample may be achieved by rotating the sample. The system we built achieves all three of these requirements. A photo of this system, attached to the ion beam line in the Cambridge Laboratory for Accelerator-based Surface Science (CLASS) at MIT, is shown in Figure 6.

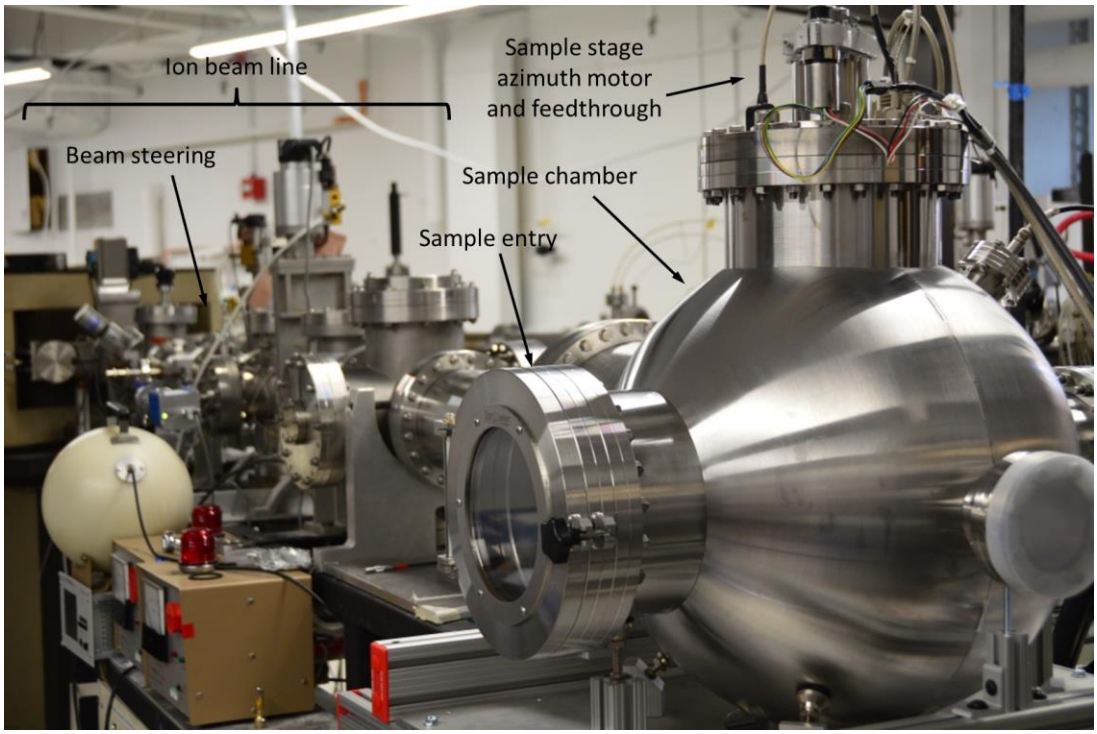

Figure 6. Photo of implant chamber mounted to the CLASS accelerator beam line, showing components after the accelerator and focusing optics. The beam is steered using electro-static steering plates, onto a sample mounted to the 2-axis sample stage in the sample chamber.

We have developed tools to write implantation machine-language programs to load onto the sample stage controllers. This process involves the following steps: 1) Calculate the stress field required to correct a measured surface error; 2) Calculate all possible ion doses and beam angles that result in the desired stress state; 3) Search for a viable continuous path; and 4) Write a machine-language program to implement the calculated path.

3.1 Implantation system layout

The implantation system consists of: 1) an ion accelerator that generates a stable beam with energy up to 10 MeV; 2) electro-magnetic focusing optics; 3) electro-static steering plates; and 4) a sample stage. We manually generate a stable ion beam and focus it to ~2 mm RMS diameter on the target. The implantation system controller controls the steering plates and the sample stage to implement a pre-calculate implant recipe (described in the following sections).

The beam steering plate potentials are driven by 5 kV bi-polar amplifiers, and given the current distance to the sample, we are able to steer the beam over an area larger than 100 mm x 100 mm. This does not significantly affect the beam profile. We are able to map the steering plate voltages to the beam position on the sample by running a program to steer the beam and take images on an alumina target (which fluoresces when hit with the ion beam). A sample image is shown in Figure 7.

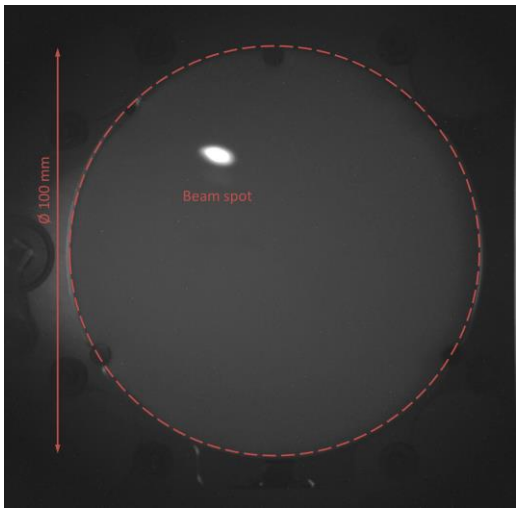

Figure 7. Sample image of a ceramic target (outline marked in red) fluorescing at the beam spot location. Images like this are used to map the ion beam positions to steering plate voltages.

The sample stage includes 2 axes of rotation, an azimuth axis and an elevation axis. The azimuth axis is powered from a motor in atmosphere via a ferro-fluid rotary feedthrough. The elevation axis is powered by a vacuum-compatible motor located in the vacuum chamber. Each axis has an encoder with an angular resolution of < 10 μrad. The unity-gain crossover frequency of each axis has been tuned to f_c > 10 Hz, which easily allows a 100 msec 5° step. The sample stage, prior to installation, is shown in Figure 8.

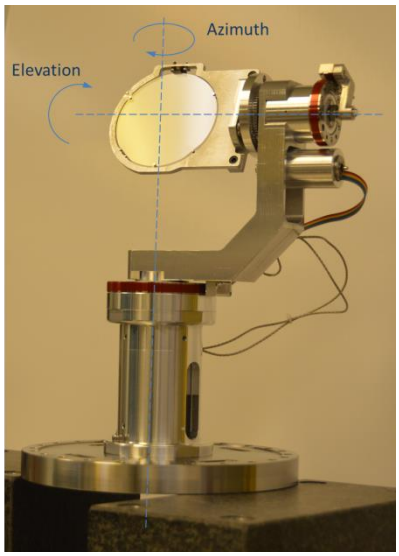

Figure 8. Sample stage during assembly. The stage is mounted on the chamber inverted from the orientation shown here. The stage is designed to accommodate substrates up to 130 mm x 200 mm.

The sample stage is required to move the sample, on one side, to angles of incidence up to 45 degrees, as well as all clocking angles. The sample stage must also be able to rotate the sample >180 degrees to implant the back side at normal-incidence. These angles are described in Section 3.3.

The third component required by the controller is a measurement of the beam flux. In order to implant the proper dose at each location, it is necessary to integrate the current hitting the target at each location. The beam current may be measured using a picoammeter capable of measuring nA to μA currents. However, for each high-energy ion hitting the sample, many secondary electrons are ejected. Since negative charges leaving the sample are indistinguishable from positive charges impacting the sample, and since the electron emission depends on the ion angle, and surface properties, we choose to suppress the electron emission by biasing the sample at +500 V. With the sample at a positive potential relative to the vacuum chamber walls, most ejected electrons return to the sample, but the bias will have a negligible effect on the incoming ~MeV ions. However, it is critical that the ion beam always hit the sample or sample holder, because any electrons emitted from other surfaces (e.g. the chamber walls) will be attracted to the sample, introducing large errors in the beam current measurement.

3.2 Calculating required correction stress states

As described previously[7], the stress generated by 6 MeV O^{3+} ion implantation into Schott D-263 glass is highly dependent on the angle of incidence of the ion beam. Integrated stress data, derived from in-situ curvature measurements[7], for normal-incidence and 45° angle of incidence implants are shown in Figure 9. For normal-incidence implants, the integrated stress in the x direction (parallel to the projection of the beam onto the surface) and the integrated stress in the y direction (perpendicular to the projection of the beam onto the surface) are nearly equal. For 45° angle of incidence, the stresses are very different. Note that in both of these samples, the twist curvature is also measured, and is found to be insignificant, indicating that xy shear stress is not significant, as expected. For Schott D-263 in particular, there is also a short-term relaxation process that occurs over hours, which affects the equi-biaxial stress primarily (i.e., the relaxation stress is nearly the same in all directions). We are able to measure this, and account for it when calculating the desired doses to implant.

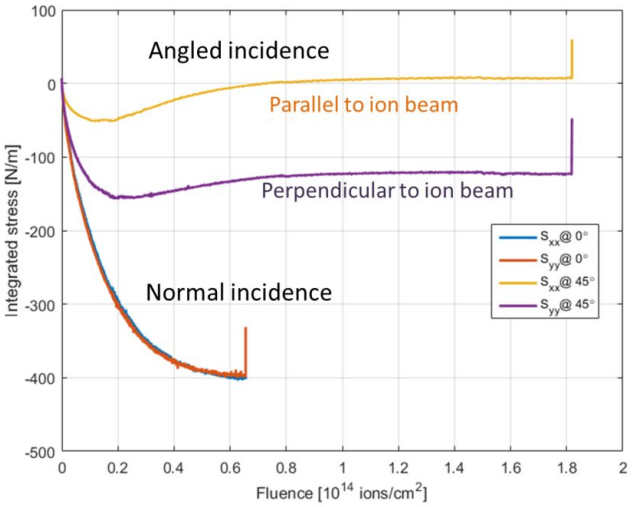

Figure 9. Integrated stress from ion implantation of Schott D-263 glass with 6 MeV O^{3+} ions. The vertical lines at the right are due to a relaxation process occurring over hours after the ion beam is turned off.

For a given figure error, we may calculate the required stress state using modal decomposition, as described previously[7]. We apply a set of test functions, record the resulting displacements, and deconvolve these displacements from the desired displacement field (i.e., the opposite of the figure error) to obtain the required stress. However, since we now have access to both equibiaxial and non-equibiaxial stress, we must test three independent stress states. In our current work we have chosen a set consisting of: an equibiaxial stress state, an anti-biaxial stress state, and a pure shear. These are shown in Figure 10.

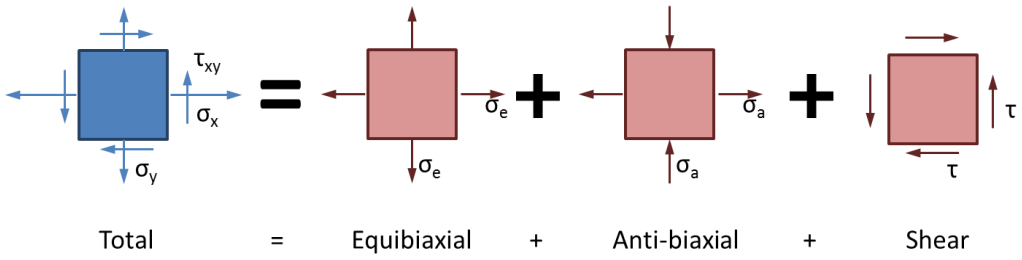

Figure 10. Set of stresses used in the current work to represent total stress state.

3.3 Possible implant angles and doses

It is helpful to explain how we convert from a required stress state to a stress state that we can implant. Figure 11 illustrates the following. The total stress, in blue, is the required stress state, consisting of two normal stress and one shear stress component at each point on the substrate. This is represented *in a particular coordinate system*, which we call the substrate coordinate system. There exists a coordinate system for which the shear stress disappears; the remaining stress components are the principle stresses, in green. Since a normal-incidence ion beam produces an equibiaxial stress state, a convenient decomposition of the principle stresses is into a uniaxial stress and an equibiaxial stress, both shown in red. The angle of coordinate rotation is referred to here as the clocking angle. The ion beam only affects the principle stresses, so the ion beam should be rotated by the clocking angle relative to the substrate coordinate system.

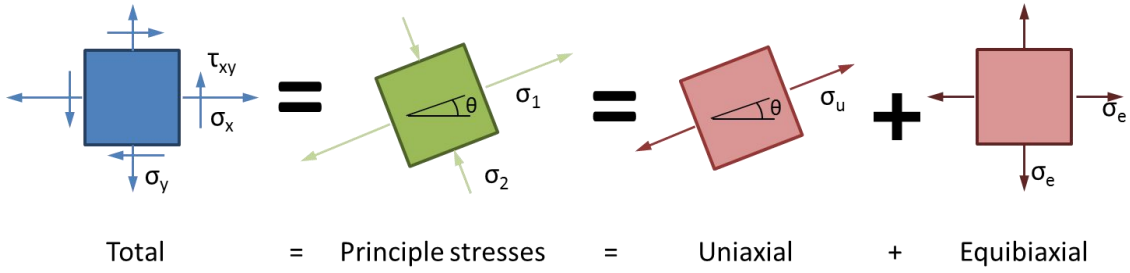

Figure 11. Set of stresses used in the current work to represent total stress state.

Looking at the experimental integrated stress data (see Figure 9), the two stresses, S_x and S_y, are the principle stresses. The uniaxial stress is the difference between the two, and equibiaxial stress is the more negative principle stress. For each position on the substrate, we may now implant at a non-zero angle of incidence to achieve the required uniaxial stress, but this has an associated equibiaxial stress. On the other side of the substrate, we may implant at normal incidence to achieve the required equibiaxial stress. Within the limits of stress magnitude that can be achieved, there are many possible ion doses and angles that result in the desired stress state.

3.4 Path calculation and machine-language programming

As stated above, there are many ion angles of incidence and associated doses on the front and back of the substrate that result in the desired stress state at each point. The possible angles of incidence and clocking angles may then be represented as an azimuth and elevation angles. However, the sample stage does not have the capability to change azimuth or elevation angles infinitely fast, and any time spent at the wrong angle will introduce error. For a given ion beam flux and measured sample stage dynamics, we may estimate the maximum allowable angle change between adjacent points on the path. We then use the A* algorithm[12] to find the path minimum dose that remains within the angle change limits.

Once a set of sample angles are found, we may calculate the required ion beam steering plate voltages, sample stage coordinates, and ion doses at each point on the substrate. At this point we can generate a machine-language program to run on Aerotech Ensemble MP controllers that control both the beam steering plates and the sample stage. Currently, the motion path is defined only at discrete points for simplicity, but in principle this could become a continuous path.

4. FUTURE WORK

We currently have all of the necessary equipment to slump, measure, and correct flat substrates. We have begun testing on the implanter system on 100 mm diameter Schott D-263 wafers and expect to finish the commissioning and tuning of the system shortly. We will likely need to continue improving the system accuracy to achieve sufficiently accurate corrections.

We will continue work on modeling the gas bearing slumping process to inform a curved-bearing slumping tool design. We also intend to begin attempting to correct curved substrates, which requires collaboration with other groups, and/or building our own capability to measure and slump curved substrates.

Other substrate materials, such as silicon, are becoming increasingly important to consider. We intend to test different thin film materials applied to silicon, such as thermally-grown silicon dioxide, to attempt to find a set of conditions that lead to non-equibiaxial stress.

6. CONCLUSIONS

We have made progress in understanding the gas bearing slumping process, and we have learned valuable information for designing a curved slumping tool that will quickly produce glass substrates with better figure error.

We have built an ion implantation system capable of controlling the beam location, ion dose, and ion beam angles on a sample up to 100 mm x 100 mm. With our current process we expect to be able to slump, measure and correct 100 mm Schott D-263 wafers.

ACKNOWLEDGEMENTS

The authors would like to thank Will Zhang, Jay Fucetola, and Alex Bruccoleri for helpful discussions. This work has been financially supported by the NASA APRA grant NNX14AE76G, the MIT Kavli Institute Research Investment Fund, and the National Science Foundation Graduate Research Fellowship Program.

REFERENCES

[1] M. C. Weisskopf, J. Gaskin, H. Tananbaum, and A. Vikhlinin, "Beyond Chandra: the x-ray Surveyor," in *Proceedings of SPIE*, 2015, vol. 9510, p. 951002.

[2] W. W. Zhang, M. P. Biskach, V. T. Bly, J. M. Carter, K. W. Chan, J. A. Gaskin, M. Hong, B. R. Hohl, W. D. Jones, J. J. Kolodziejczak, L. D. Kolos, J. R. Mazzarella, R. S. McClelland, K. P. McKeon, T. M. Miller, S. L. O'Dell, R. E. Riveros, T. T. Saha, M. J. Schofield, M. V. Sharpe, and H. C. Smith, "Affordable and lightweight high-resolution x-ray optics for astronomical missions," in *Proceedings of SPIE*, 2014, vol. 9144, p. 914415.

[3] M. L. Schattenburg, B. Chalifoux, M. D. DeTienne, R. K. Heilmann, and Heng Zuo, "Progress report on air bearing slumping of thin glass mirrors for x-ray telescopes," in *Proceedings of SPIE*, 2015, vol. 9603, p. 96030R.

[4] A. Winter, E. Breunig, P. Friedrich, and L. Proserpio, "Progress on indirect glass slumping for future x-ray telescope optics," in *Proceedings of SPIE*, 2014, vol. 9144, p. 91441C.

[5] R. Allured, S. Ben-Ami, V. Controneo, V. Marquez, S. McMuldroch, P. B. Reid, D. A. Schwartz, S. Trolier-McKinstry, A. A. Vikhlinin, M. L. Wallace, "Improved control and characterization of adjustable x-ray optics," in *Proceedings of SPIE,* 2015, vol. 9603, p. 96031M.

[6] M. P. Ulmer, X. Wang, J. Cao, J. Savoie, B. Bellavia, M. E. Graham, and S. Vaynman, "Progress report on using magneto-strictive sputtered thin films to modify the shape of a x-ray telescope mirror," in *Proceedings of SPIE*, 2012, vol. 8503, p. 85030C.

[7] B. Chalifoux, G. Wright, R.K. Heilmann, M.L. Schattenburg, "Ion implantation for figure correction of thin x-ray telescope mirror substrates," in *Proceedings of SPIE*, 2015, vol. 9603, p. 96031K.

[8] C. Atkins, K. Kilaru, B. D. Ramsey, D. M. Broadway, M. V. Gubarev, S. L. O'Dell, W. W. Zhang, "Differential deposition correction of segmented glass x-ray optics," in *Proceedings of SPIE*, 2015, vol. 9603, p. 96031G.

[9] D. Windt, R. Conley, "Two-dimensional differential deposition: figure correction of thin-shell mirror substrates for x-ray astronomy," in *Proceedings of SPIE*, 2015, vol. 9603, p. 96031H.

[10] S. Klaumünzer, "Ion tracks in quartz and vitreous silica," *Nucl. Instrum. Methods Phys. Res. Sect. B Beam Interact. Mater. At.*, vol. 225, no. 1–2, pp. 136–153, Aug. 2004.

[11] C.R. Forest, C.R. Canizares, D.R. Neal, M. McGuirk, M.L. Schattenburg, "Metrology of thin transparent optics using Shack-Hartmann wavefront sensing," Opt. Eng. 43(3) 742-753 (2004).

[12] S. M. LaValle, *Planning Algorithms*, Cambridge University Press, 2006.